Optical Pumping: Characterizing the Hyperfine Structures, Zeeman Interactions and Nuclear Spins of ^{85}Rb and ^{87}Rb

Ian Haines*
Department of Physics, University of California, Berkeley, 366 Physics North, Berkeley, CA 94720
(Dated: November 7, 2023)

Determining the structure of atoms as well as their interactions with light is important for a further understanding of physics. One way to determine this structure is through optical pumping. Optical pumping was performed on ^{85}Rb and ^{87}Rb. The Breit-Rabi formula which gives the Zeeman resonances was confirmed following a weighted linear regression and analysis of the results. The nuclear spins were determined to be $I_{85} = 2.56 \pm 0.13$ and $I_{87} = 1.54 \pm 0.77$. Earth's magnetic field was also determined. Two methods were used to determine the field strength. One method was determined to be more robust giving 431 ± 22 gauss. The pumping time was determined to be 25 ± 10 ms. Analysis of all results included as well as figures and fit parameters along with uncertainties.

Keywords: Optical pumping, Breit-Rabi, hyperfine, zeeman, spectroscopy, nuclear physics, atomic physics

I. INTRODUCTION

Spectroscopy, the branch of physics concerning the interactions between matter and light, has been a topic of interest for physicists for centuries going back to Isaac Newton's studies of sunlight dispersing within a glass prism [1]. Quantum mechanics provides a systematic way to study these interactions at small scales that classical physics cannot provide. One of the earlier insights furnished by quantum mechanics was the notion that atomic transitions from one bound state to another happen only when a fixed, specific amount of energy is either absorbed by or emitted from an atom so that all transitions between bound states compose a discrete spectrum [2]. The structure of atoms and their interactions can be understood then by a complete understanding of the transitions between bound states.

One way of forcing these atomic transitions is through a method called optical pumping. Specifically, the structure of alkali atoms, in particular ^{85}Rb and ^{87}Rb, can be elucidated via optical pumping [3]. Optical pumping works by subjecting a gas of Rb atoms to a magnetic field to create a preferred direction of quantization and then an electromagnetic radiation field to "pump" the gas away from an equilibrium distribution towards a nonequilibrium one which becomes transparent to the radiation eventually. These atoms are termed "optically dark" to the radiation field. By applying a radiofrequency (rf) field, the atoms can be broken out of their degenerate states back to a new equilibrium distribution which is opaque to the light again. This technique is called Optically Detected Magnetic Resonance or ODMR since the rf frequency is a resonant frequency of the Zeeman transitions. This technique is used to determine the nuclear spin of the atom since the rf field interaction depends upon the value of this quantity. Additionally, this technique is also used to verify the calculated resonant Zeeman transitions and the Breit-Rabi formula.

The magnetic field interactions with the atoms are treated through perturbation theory. The application of perturbation theory is best understood in the context of the vector model of angular momenta. The radiation field interaction is treated by finding which matrix elements of the dipole operator are non-zero. These non-zero elements say which transitions from $|a\rangle \to |b\rangle$ are allowed.

A. Vector Model of Angular Momenta

In ^{85}Rb and ^{87}Rb, henceforth Rb will refer to both isotopes unless otherwise specified, there are 36 electrons bound to the nucleus due to the Coulomb interaction and one valence electron in the $5s$ orbital. This electron can be specified by its spin angular momentum and orbital angular momentum, $\mathbf{S}$ and $\mathbf{L}$, respectively, where $S = \frac{1}{2}$ and $L = 0, 1, 2, ...$ The total electronic angular momentum is given by their sum $\mathbf{J} = \mathbf{L} + \mathbf{S}$. The rules of the addition of angular momenta yield $J = \frac{1}{2}, \frac{3}{2}, \frac{5}{2}, ...$ In addition to this, the nucleus of Rb also has a spin angular momentum denoted $\mathbf{I}$; and, $I = \frac{5}{2}$ for ^{85}Rb and $I = \frac{3}{2}$ for ^{87}Rb. The total angular momentum of Rb is therefore given by the sum $\mathbf{F} = \mathbf{I} + \mathbf{J}$. The rules of the addition of angular momenta yield $F = 1, 2, ...$ [2].

B. Sketching the Perturbation Scheme

1. *Energy Splitting from the Intrinsic Interaction*

The hyperfine interaction occurs due to the interaction between the $\mathbf{B}$-field generated by the electronic angular momentum, and the nuclear magnetic moment,

$$\boldsymbol{\mu}_I = -g_I \mu_N \frac{\mathbf{I}}{\hbar},$$

* ianphaines@berkeley.edu

where g_I is the effective g-factor of the nucleus and μ_N is the nuclear magneton. The Hamiltonian has the form

$$\hat{\mathcal{H}}_{\text{hfs}} = -\boldsymbol{\mu}_I \cdot \mathbf{B}_J \propto \mathbf{J} \cdot \mathbf{I} \tag{1}$$

which splits the energy eigenvalues arising from the fine structure interaction (see Fig's 1 and 2). This splitting is due to the $(2S+1) \times (2L+1) \times (2I+1)$ combinations between the total electronic orbital angular momenta and nuclear spin eigenstates.

Using the fact that $\mathbf{F} = \mathbf{J} + \mathbf{I}$, 1 can be rewritten as

$$\hat{\mathcal{H}}_{\text{hfs}} \propto \frac{1}{2}(F^2 - J^2 - I^2) \tag{2}$$

implying that the desired basis to evaluate this term is the coupled basis. The eigenbasis vectors are given by $|I, J; F, m_F\rangle$ where $m_F = -F, -F+1, \cdots, F-1, F$. These states can be obtained using the Clebsch-Gordan coefficients and the uncoupled basis vectors $|I, m_I; J, m_J\rangle$.

2. Zeeman Splitting in the Hyperfine Perturbation

In the presence of an external magnetic field whose wave vector is oriented parallel to the axis of quantization, the nuclear magnetic moment and electronic magnetic moment have a tendency to precess about the direction of motion of the field. As a result, the hyperfine structure Hamiltonian becomes

$$\hat{\mathcal{H}}_{\text{hfs+B}} = -\boldsymbol{\mu}_I \cdot (\mathbf{B}_J + \mathbf{B}_{\text{ext}}) - \boldsymbol{\mu}_J \cdot \mathbf{B}_{\text{ext}} \tag{3}$$

where $\mathbf{B}_{\text{ext}}$ is the external magnetic field and

$$\boldsymbol{\mu}_J = g_J \mu_B \frac{\mathbf{J}}{\hbar}$$

is the magnetic moment of the electronic angular momentum where g_J is the Landé g-factor. The equation 3 can be rewritten as

$$\hat{\mathcal{H}}_{\text{hfs+B}} = \hat{\mathcal{H}}_{\text{hfs}} + \hat{\mathcal{H}}_{\text{B}} \tag{4}$$

where $\hat{\mathcal{H}}_{\text{B}} = -(\boldsymbol{\mu}_I + \boldsymbol{\mu}_J) \cdot \mathbf{B}_{\text{ext}}$. In the limit where $\mathbf{B}_{\text{ext}}$ goes to zero, 1 is recovered.

C. The Weak Field Breit-Rabi Formula

In the case of optical pumping, the field is weak enough so that the hyperfine energies dominate the external field term [5]. Thus, the field term can be treated as a perturbation. The hyperfine Landé g-factor is given by

$$\begin{aligned} g_F = g_I &\frac{F(F+1) + I(I+1) - J(J+1)}{2F(F+1)} + \\ g_J &\frac{F(F+1) - I(I+1) + J(J+1)}{2F(F+1)} \\ \approx g_J &\frac{F(F+1) - I(I+1) + J(J+1)}{2F(F+1)} \end{aligned} \tag{5}$$

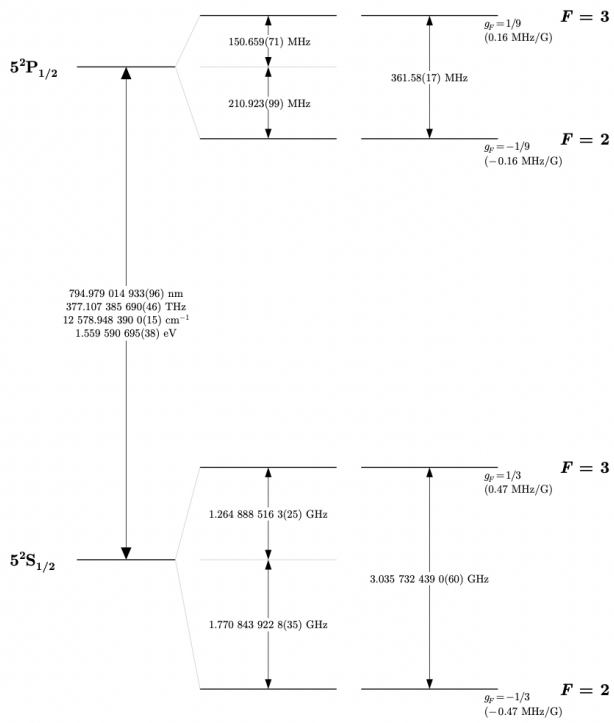

FIG. 1: ^{85}Rb D1 transitions for the hyperfine structure. Spacings for the hyperfine structure are scaled for those energies only and shouldn't be compared to the optical spacing. Figure taken from [4]

since $g_I \ll g_J$. Consequently, the second term in 4 can be rewritten as

$$\hat{\mathcal{H}}_{\text{B}} = g_F \mu_B \frac{\hat{F}_z}{\hbar} B_z. \tag{6}$$

In this case, the coupled basis is still a good basis to use to calculate the energy eigenvalues.

Applying 6 then yields the low-field Breit-Rabi formula

$$E_{F,m_F} = g_F \mu_B m_F B_z \tag{7}$$

In the electronic ground state, $F = I + \frac{1}{2}$, so

$$E_{F,m_F} = \frac{m_F \mu_B g_J}{2I+1} B_z$$

Hence, the energy differences for which $\Delta m_F = \pm 1$ are given by

$$h\nu = \frac{\mu_B g_J}{2I+1} B_z \tag{8}$$

where ν is the frequency of the rf field.

D. Optical Pumping and Selection Rules

The radiation field is characterized by a polarization vector $\hat{\boldsymbol{\epsilon}} = \epsilon^+ \hat{\sigma}^+ + \epsilon^- \hat{\sigma}^-$ where the polarization basis

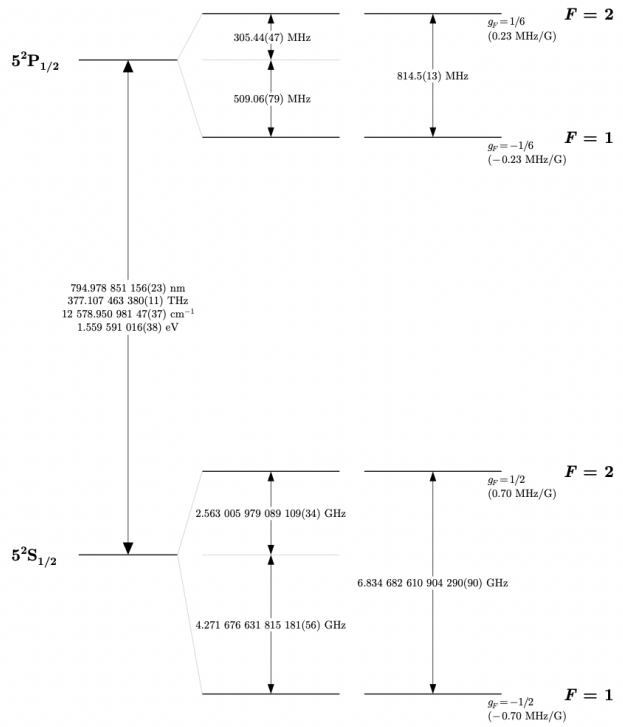

FIG. 2: ^{87}Rb D1 transitions for the hyperfine structure. Spacings for the hyperfine structure are scaled for those energies only and shouldn't be compared to the optical spacing. Figure taken from [5]

consists of $\hat{\sigma}^+$ corresponding to right-handed circularly polarized light and $\hat{\sigma}^-$ corresponding to left-handed circularly polarized light and both vectors are orthogonal to the axis of quantization.

Without the radiation field, the atoms have an thermal equilibrium distribution of their m_F values corresponding to the ambient temperature of the bulb. When the radiation field is turned on, the interaction between the field and the atoms can be described by the dipole operator

$$\hat{d} = \hat{\boldsymbol{\epsilon}} \cdot \hat{\mathbf{r}} \tag{9}$$

where $\mathbf{r}$ is the position vector of an atom. In the case of only right-handed polarization, the atoms are cyclically driven to a new distribution where $m_F = +2$ [5]. At this point, the atoms become transparent to the light and it is as if there is no gas there in the radiation field. This change can be measured via an oscilloscope connected to a photodetector.

E. Pumping Time

It has been noted already that when the rf field interacts with the pumped gas that it knocks the gas out of the pumped state. How long does it take then for the unpumped gas to become pumped again? In principle, this can be answered by knowing the rate of transition between each of the states as a function of time. Since the radiation field causes the transition, the transition will depend upon the matrix element $\hat{D}_{ba}$ where $\hat{D}$ is the dipole operator and b and a are states with $m_F = b$ and $m_F = a$ respectively. Steck has given the matrix element values [4][5] for both ^{85}Rb and ^{87}Rb.

In addition to this, the problem can be treated as one of a sudden perturbation in the Hamiltonian. In this case, the radiation field is a small perturbation that is time independent. So, the probability amplitudes can be determined from time-independent perturbation theory. The first order transition probability (denoted by the $^{(1)}$) is given by [6]:

$$P_{ba}^{(1)}(t) = \frac{2}{\hbar^2}|\hat{D}_{ba}|^2 \frac{2\sin^2(\omega_{ba}t/2)}{\omega_{ba}^2} \tag{10}$$

where $\omega_{ba} = (E_b - E_a)/\hbar$ is the Bohr angular frequency or frequency difference of the unperturbed states b and a.

Outside of the scope of this paper is the density matrix formalism which must be used to determine what the actual population values are of the states as a function of time. Again, [6], discusses this formalism and how to calculate the time rate of change of the density of states.

II. EXPERIMENTAL METHODS

A. Overview of the Apparatus

As alluded to in the introduction, the necessary components for observing ODMR are an atomic cell containing Rb gas, a strong magnetic field source, a radiation field source, an rf field source, and a photodetector. A block diagram can be found in Fig. 3 taken from [7].

The Helmholtz coil serves as the magnetic field source which creates the axis of quantization. The radiation source emits a field which passes through the atomic vapor cell and strikes the photodetector. The signal detected is amplified by an amplifier and sent to an oscilloscope for observations. Meanwhile, the rf field generator generates a field which continually knocks the pumped gas back into an unpumped state thereby stimulating emission of the D1 transition line. This allows for the continual viewing of the pumping and de-pumping corresponding to Zeeman resonances on the oscilloscope.

B. Overview of the Procedure

1. General Idea

The Helmholtz coil field strength, B_{HH}, can be found using the Biot-Savart law for a magnetic field of N current

loops:

$$B = \left(\frac{4}{5}\right)^{\frac{3}{2}} \frac{\mu_0 N I}{R} \tag{11}$$

where μ_0 is the permittivity of free space, N is the number of loops, I is the current, and R is the radius of the coil.

Using the weak field Breit-Rabi formula in 7, the resonant frequencies can be calculated by solving for ν and using the Helmholtz coil field strength. Thus, the resonant frequency of the Zeeman transitions and hence rf field can be found for any value of B_{HH}.

By applying a sinusoidal current to the rf generator and sweeping through a range of frequencies which covers the resonant frequencies for both ^{85}Rb and ^{87}Rb given a certain B_{HH}, ODMR can be observed (see Fig. 4).

Another method to observe the ODMR is to fix the frequency of the rf field and change the strength of the Helmholtz coil field. This method is known as lock-in detection since it is used to extract the signal in spite of the noise within the environment. By carefully adjusting the Helmholtz coil field and switching the settings on the oscilloscope so that it displays a polar representation of the signal, Fig. 5 can be observed.

In addition to viewing ODMR, the timescales for optical pumping can be observed. The rf generator can be configured to generate a sinusoidal wave whose amplitude is modulated by a square wave. By configuring the oscilloscope to trigger at the proper times, Rabi oscillations can be observed as the spins re-orient themselves (see Fig. 6).

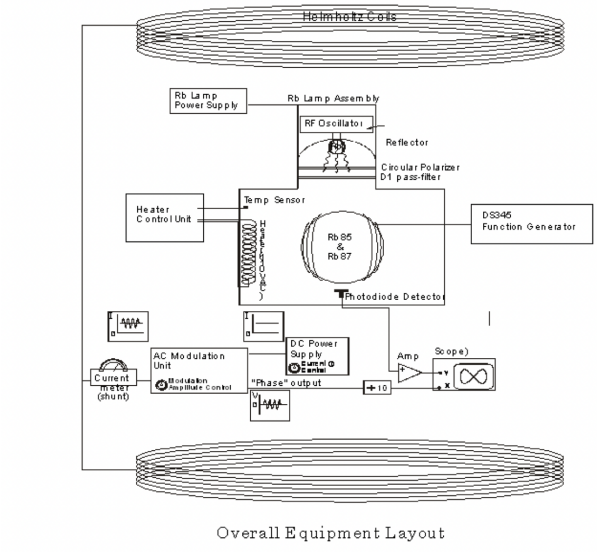

FIG. 3: Block diagram for the optical pumping technique. Included are all of the elements necessary to observe ODMR using optical pumping. Important to note is that the specific equipment is not necessary.

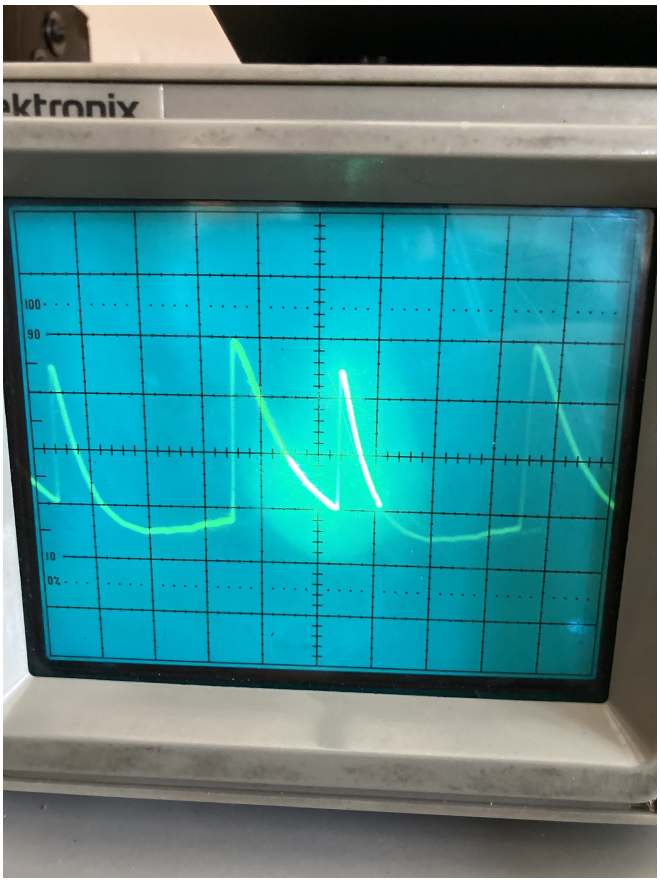

FIG. 4: Oscilloscope display of ODMR: the first observed sharp spike in the middle of the screen occurs when the $\nu_{\text{rf}} = \nu_{\text{Zeeman}}$ for ^{85}Rb since it has $I = 5/2$ while the second spike occurs when $\nu_{\text{rf}} = \nu_{\text{Zeeman}}$ for ^{87}Rb since it has $I = 3/2$

2. *Subtleties Involved*

Important to note is that the field within the atomic vapor cell will not be exactly equal to the field due to the coil. Earth's ambient magnetic field is on the order of 0.25 to 0.65 gauss [8]. For a coil with $N = 135$, $I = 1$A, and $R = 27.5$cm, $B \approx 4.4$ gauss.

Another important aspect to note is that the heater used to excite the Rb atoms into a gas generates a magnetic field. The thermal radiation field is generated via resistive heating in a coil. Due to a changing electric field within the coil, Faraday's law states that a time-varying magnetic field is generated. Unlike Earth's ambient field, this field can be removed by turning the radiation field generator off while observing ODMR. The current dissipates within the coil on a timescale much faster than the ambient field generated by the coil within the vapor cell decreases and so ODMR can still be viewed for some time after the coil is turned off.

A final note is that the temperature within the cell must be selected properly so as to get equal amounts of ^{85}Rb and ^{87}Rb gas. This can be done by looking at

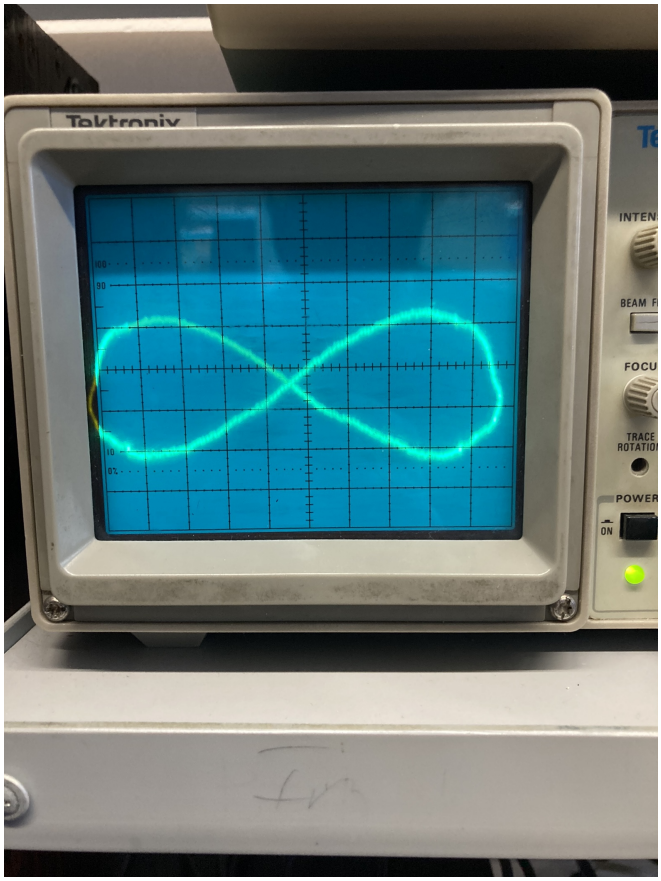

FIG. 5: Oscilloscope display of ODMR using the lock-in detection method. A strong resonant signal will display an evenly symmetric lemniscate that is not pinched on the sides.

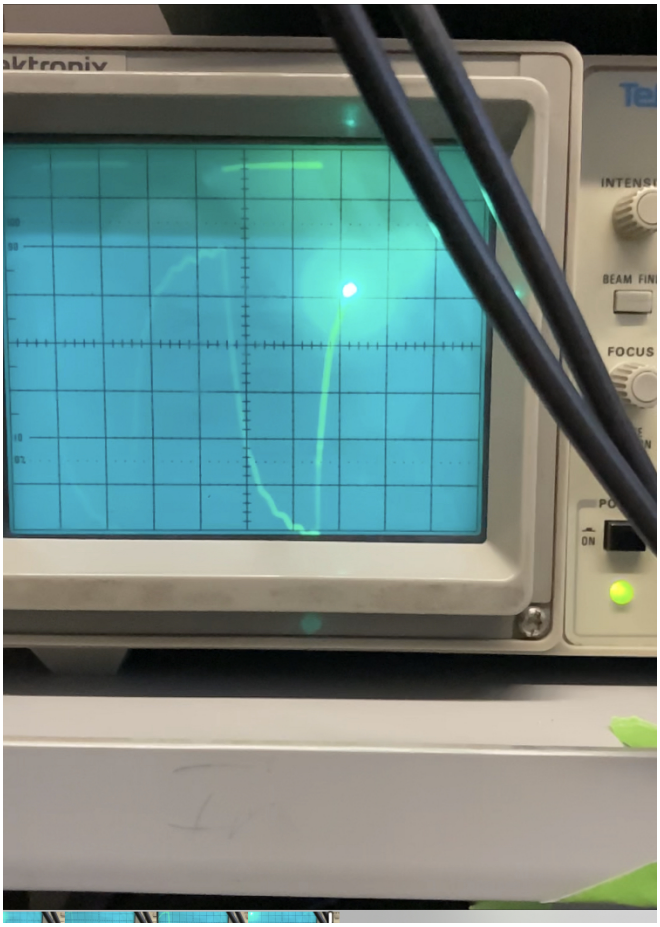

FIG. 6: Oscilloscope display of Rabi oscillations and spin re-alignment. The time it takes to pump can be measured by how long it takes for the signal to decay back down to zero.

the optical signal amplitude as a function of time for the gas for both isotopes. For a Rb mixture, the optimal temperature seems to be $\sim 50C^{\circ}$ (see Fig's 7).

III. RESULTS AND ANALYSIS

The resonant frequencies were calculated for currents on the interval $[-3.0\text{ A}, 3.0\text{ A}]$ in steps of 0.5 A. From these frequencies, the currents were varied until the clearest resonance picture displayed on the oscilloscope (see Fig. 5). The frequencies as well as the nominal and real current values can be found in Table 1.

A. Testing the Breit-Rabi Formula

The data followed a linear relationship for both isotopes. A weighted least squares had been performed on four different sets of data: the negative current data for both isotopes and the positive current data for both isotopes (See Fig's 8-11). The slopes for positive and negative polarities for one isotope differed by roughly 2 percent. A weighted linear regression could be run just once for each isotope by combining the two polarity datasets into one for each isotope, but since this difference in slopes is so small this is unnecessary. The vertical intercept value differed across isotopes. This could possibly indicate that the method is not robust, but it could also indicate that the ambient field generated was not constant during measurements (see subsection C below).

The main source of errors in determining these resonances were the difficulties in determining which lemniscate figure on the oscilloscope was the most symmetric about the horizontal and vertical axes and the ambient magnetic field within the atomic vapor cell. Trying to quantify the error due to the oscilloscope is rather difficult since there is no systematic method to determine the symmetry of the figure within the laboratory.

The error in the current measurement is most likely negligible because the shunt resistor used to measure the current through the coil is well calibrated and the percent change in resistance per degree in C° is given by $\frac{\mathrm{d}R}{\mathrm{d}T}/R = 0.002\%\ \mathrm{T}^{-1}$. In this case, however, it was assumed that

TABLE I: All currency values are reported with an error of 1%. The errors of the resonant frequencies are determined using the formula given in equation 12.

I_{nominal} [A]	^{85}Rb I_{real} [A]	^{85}Rb ν [MHz]	^{87}Rb I_{real} [A]	^{87}Rb ν [MHz]
−3.0	−3.1389	6.18	−3.1259	9.27
−2.5	−2.62238	5.15	−2.61408	7.72
−2.0	−2.10796	4.12	−2.10569	6.18
−1.5	−1.59567	3.09	−1.59272	4.63
−1.0	−1.0840	2.06	−1.08500	3.09
−0.5	−0.6932	1.3	−0.5727	1.51
0	0	0.1952	0	0.3111
0.5	0.56992	1.30	0.68987	1.544
1.0	0.94427	2.06	0.94563	3.09
1.5	1.450	3.09	1.45163	4.63
2.0	1.95087	4.12	1.95911	6.18
2.5	2.45401	5.15	2.46186	7.72
3.0	2.9520	6.18	2.9689	9.27

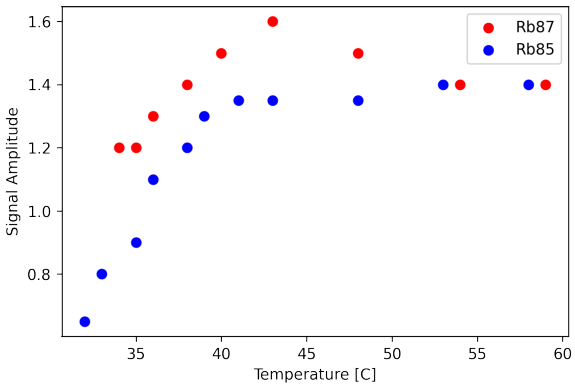

FIG. 7: Signal strength as a function of temperature. The importance of this is to see the vaporization as a function of temperature. It needs to be approximately equal for the gas to be equal parts of both isotopes.

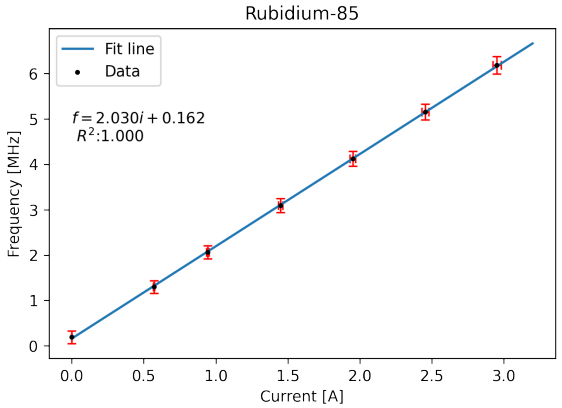

FIG. 8: Positive polarity ^{85}Rb data along with the WLS regression line.

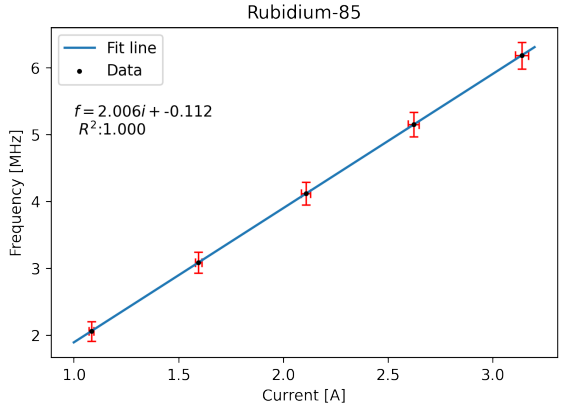

FIG. 9: Reversed polarity ^{85}Rb data along with the WLS regression line.

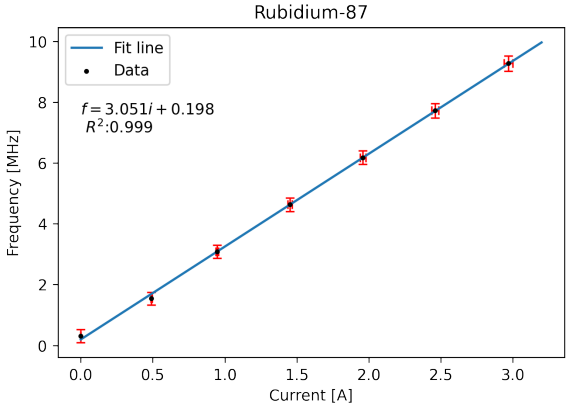

FIG. 10: Positive polarity ^{87}Rb data along with the WLS regression line.

there is a gaussian distribution about each current that generates a 1% error in the measurement. This error

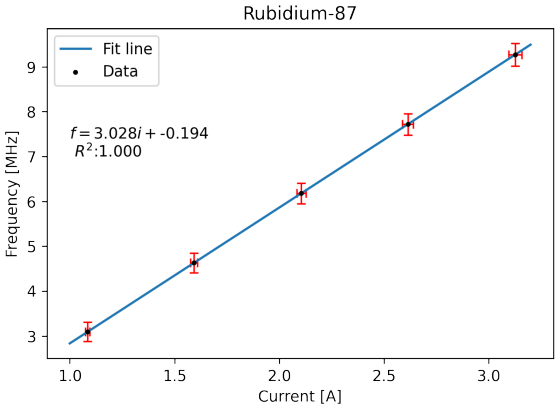

FIG. 11: Reversed polarity ^{87}Rb data along with the WLS regression line.

is propagated throughout the frequency calculation thus giving a current dependent error.

There are other possible sources of error such as the error in the magnitude of the radius of the coil. This error was found to be negligible relative to the possible error arising from the current and so can be ignored. Another possible source of error that is beyond the scope of this paper in quantifying is the error associated with the geometry of the Helmholtz coil itself. The Helmholtz field magnitude formula assumes that the coils are idealized and that the wires are wrapped identically in both coils. There are small fluctuations in the field due to the imperfections in the geometry of the wound wires. The error associated with this could be addressed in future efforts.

The ambient field within the atomic cell was calculated using a prior given in [8] which quotes an average ~ 0.3 gauss at Berkeley's latitude and longitude. This error, σ_B, can be converted into a frequency error, σ_f, using the Breit-Rabi formula in equation 7. Both of these errors are represented by errorbars on the plots in Fig's 7-10.

The total uncertainty is given by the equation

$$\sigma_\nu = \frac{2.799}{2I+1}\sqrt{\left[\left(\frac{4}{5}\right)^{3/2}\frac{\mu_0 n}{R}\right]^2 \sigma_i^2 + \sigma_{B_\oplus}^2} \tag{12}$$

where σ_i is the uncertainty in the current and $\sigma_{B_\oplus}$ is the ambient magnetic field of the earth.

The weak field Breit-Rabi hypothesis cannot be rejected due to the robustness of the linear regressions. Each regression determined an R^2 value of ≈ 1 and since this model has only 2 parameters and more than 10 data points for each dataset, the R^2 statistic can be meaningfully interpreted as a goodness-of-fit statistic.

B. Determining I_{85} and I_{87}

One approach to determine the values of I_{85} and I_{87} is by taking the ratio of the resonant frequencies ν_{85}/ν_{87} and using that to determine the ratio of the nuclear spins. This method suffers from the error of having the ambient field contribute to the magnetic field sum. A more robust method can be done by taking the ratio of the difference of two resonant frequencies for two given currents:

$$\frac{\nu_{85}^1 - \nu_{85}^2}{\nu_{87}^1 - \nu_{87}^2} = \frac{(i_{HH}^1 - i_{HH}^2)_{85}}{(i_{HH}^1 - i_{HH}^2)_{87}} \cdot \frac{2I_{87}+1}{2I_{85}+1} \tag{13}$$

where i_{HH} is the current of the Helmholtz coil. This method eliminates the ambient field and also allows for the cancellation of various factors such as coil radius, etc. The uncertainty can be obtained by propagating the uncertainties in the resonant frequencies and currents using the formulae given in [9]. This method can be used instead of the simple ratio method because the relationship between frequency and current is linear according to the Breit-Rabi formula. The values obtained can be found in Table II. From this ratio alone, the values of I_{85} and I_{87} cannot be deduced since the ratio depends on both spin values. In the event that one of the spin values were known, then the other could be determined.

TABLE II: The ratio is determined as an average value by iterating through each difference generated from the resonant frequency datasets. The error is obtained through considering the propagation of errors.

$\Delta\nu_{85}/\Delta\nu_{87}$	σ
0.670	1.35×10^{-2}

Another method to determine the nuclear spins is by using the fit parameters obtained in the linear regressions. This is done by taking the slope of each line and deducing what the value of I_{85} and I_{87} must be using the Breit-Rabi equation and the Helmholtz coil field strength equation. The values obtained from this method (see Table III) show rough agreement with the theoretical values for the nuclear spins. The uncertainties obtained in this were done by propagating the uncertainties in the fit parameters. This was done by solving for the nuclear spin as a function of the slope of the line.

Although half-integral values are expected, the recorded results show that half-integral values fall outside of the uncertainties. Hence, it is possible that new physics is actually uncovered here. It is also possible that the uncertainties in the fit parameters should actually be higher. The fit parameter uncertainties are dependent upon the measured current values and their uncertainties as well as the uncertainties in the resonant frequencies. Thus, if any of these uncertainties or values are invalid, the uncertainty analysis here would be invalid.

C. The Ambient Field

The ambient field can be obtained using two different methods: one method uses the zero-field resonance

TABLE III: Nuclear spins deduced from the linear fits obtained. The uncertainties in the fit parameters were used as uncertainties in the slopes.

I_{85}	σ_{85}	I_{87}	σ_{87}
2.58	0.161	1.54	0.097
2.54	0.0944	1.52	0.0574

and determines the value from the data while the other method determines it from the fit parameters. The field obtained from both methods can be found in Table IV.

The first method provides an estimate for the field because Earth's magnetic field is now the axis of alignment for the atoms which allows them to be pumped into an optically dark state.

The values are not consistent with each other, but they may be consistent with each other. The reasoning is as follows: Earth's magnetic field is constantly changing direction and magnitude. Earth's field may be changed by the movement of any metal objects around it or currents running through various wires.

In the first method, the error comes primarily from determining when the resonance is actually reached and so the chief error is the error in the frequency. This error is difficult to quantify, but it scales linearly when using an error propagation method and so for every change in one unit of the frequency, there is a change $\frac{2I+1}{2.799}$ units of Earth's ambient field. A liberal estimate of 5% error was chosen for propagation. An example of a resonance can be seen in Fig 4.

In the second method, the fit parameter is used to determine the strength of the ambient field. This method is less robust since the uncertainty in the intercept parameter is much higher than the uncertainty in the slope parameter. This uncertainty is propagated in the calculation for the ambient field.

TABLE IV: Column 1 contains the magnetic field calculated using the Rubidium-85 zero-field resonance. Column 2 contains the magnetic field calculated using the Rubidium-87 zero-field resonance.

$B_\oplus$[gauss]	$B_\oplus$[gauss]
418±20.9	444±22.2

TABLE V: Column 1 contains the magnetic field calculated using the Rubidium-85 fit parameters. Column 2 contains the magnetic field calculated using the Rubidium-87 fit parameters.

$B_\oplus$[gauss]	$B_\oplus$[gauss]
240 ±471	277 ±442
347 ±214	282 ±206

It might be asked why there is a zero-field resonance in the first place. Although Earth's magnetic field does fluctuate, the fluctuation can be quite small and even slow if the fluctuation is large. This means that large fluctuations only happen on a longer time scale [8]. Hence, Earth's magnetic field can create an axis of quantization within the vapor cell and allow resonances to occur.

D. Pumping Time

The pumping time is defined to be the time it takes for the optical signal amplitude to decrease by a factor of e^{-1}. It was found to be roughly 25 ± 10ms. This can be done by viewing the oscilloscope and measuring the change in the height of the signal and the change in the time it takes for that decrease in height. Since this method relies on looking at the oscilloscope trace which is inherently grainy and has a poor resolution in addition to having imprecise markings for each division, the uncertainty is rather high which is why a liberal estimate of 10ms is given.

IV. CONCLUSION

Optical pumping was performed for ^{85}Rb and ^{87}Rb isotopes to determine the hyperfine structures, Zeeman structures, nuclear spins, and optical pumping timescale. This was done by heating an atomic vapor cell to excite the rubidium into a gas and subjecting it to a weak magnetic field which broke the symmetry in the hyperfine states in addition to a radiation field which pumped the gas. The weak field Breit-Rabi formula was confirmed in the analyses as were the nuclear spins of both isotopes. The ambient magnetic field was measured, but it was more difficult to determine the actual field strength. The pumping time was also very roughly estimated. In the future, a more formal approach involving the time evolution of the density of states is warranted to determine the accuracy of the value given for the pumping time.

V. ACKNOWLEDGEMENTS

I would like to thank Rachel Wang for her patience and brilliance in determining the proper method for finding the Zeeman resonances as well as providing great insight into the theoretical nature of this experiment. I would like to also thank Luc Le Pottier for his patience in helping us calibrate the oscilloscope as well as some of the other equipment to measure some of the necessary quantities.

[1] N. C. Thomas, The early history of spectroscopy, Journal of Chemical Education **68**, 631 (1991), https://doi.org/10.1021/ed068p631.

[2] D. J. Griffiths, *Introduction to Quantum Mechanics (2nd Edition)*, 2nd ed. (Pearson Prentice Hall, 2004).

[3] R. Benumof, Optical pumping theory and experiments, American Journal of Physics **33**, 151 (1965), https://doi.org/10.1119/1.1971285.

[4] D. Steck, Rubidium 85 d line data (2021), available at: `https://steck.us/alkalidata/rubidium85numbers.1.6.pdf`.

[5] D. Steck, Rubidium 87 d line data (2021), available at: `https://steck.us/alkalidata/rubidium87numbers.1.6.pdf`.

[6] B. H. Bransden and C. J. Joachain, in *Quantum Mechanics* (Pearson/Prentice Hall, 2000) 2nd ed.

[7] *OPT - Optical Pumping*, University of California, Berkeley.

[8] C. C. Finlay, S. Maus, C. D. Beggan, T. N. Bondar, A. Chambodut, T. A. Chernova, A. Chulliat, V. P. Golovkov, B. Hamilton, M. Hamoudi, R. Holme, G. Hulot, W. Kuang, B. Langlais, V. Lesur, F. J. Lowes, H. Lühr, S. MacMillan, M. Mandea, S. McLean, C. Manoj, M. Menvielle, I. Michaelis, N. Olsen, J. Rauberg, M. Rother, T. J. Sabaka, A. Tangborn, L. Tøffner-Clausen, E. Thébault, A. W. P. Thomson, I. Wardinski, Z. Wei, and T. I. Zvereva, International Geomagnetic Reference Field: the eleventh generation, Geophysical Journal International **183**, 1216 (2010).

[9] A summary of error propagation, available at `http://ipl.physics.harvard.edu/wp-uploads/2013/03/PS3_Error_Propagation_sp13.pdf`.